PCCP

Accepted Manuscript

ROYAL SOCIETY OF CHEMISTRY

www.rsc.org/pccp

Journal Name

RSCPublishing

ARTICLE

Effects of repulsive interaction on the electric double layer of an imidazolium-based ionic liquid by molecular dynamics simulation

Wenyang Jin,†[a] Xiaohong Liu,†[a] Yining Han,‡[a] Shu Li[a] and Tianying Yan*[a]

Cite this: DOI: 10.1039/x0xx00000x

Received 00th January 2012,
Accepted 00th January 2012

DOI: 10.1039/x0xx00000x

www.rsc.org/

Effects of repulsive interaction on electric double layer (EDL) and differential capacitance (C_d) of an ionic liquid (IL) 1-butyl-3-methyl-imidazolium hexafluorophosphate ($BMIM^+/PF_6^-$) on the graphite electrode were studied by molecular dynamics (MD) simulations. The strength of repulsive interaction was studied by manually tuning the parameter lamda (λ), with λ =1.00 for normal Lennard-Jones interaction and smaller λ for stronger repulsion between IL and the electrode. When λ changes from 1.00 to 0.25, the dependence of C_d on potential (C_d-U) curves at different repulsions are asymmetric camel-shaped with higher C_d at the negative polarization than that at the positive polarization, due to the thinner effective thickness of EDL from the specific adsorption of $BMIM^+$. Such trend is opposite in the case of λ = 0.05. Apart from that, the maximum of C_d at the negative polarization monotonically decreases with increasing the repulsion. On the other hand, the maximum of C_d at the positive polarization first increase with increasing the repulsion, due to the more effective screening of PF_6^- by weakening the specific adsorption of $BMIM^+$ as λ changes from 1.00 to 0.75, and then it decreases as cases at the negative polarization.

Keywords: differential capacitance · electric double layer · ionic liquids · molecular dynamics simulation ·repulsive interaction

1. Introduction

Recently, room-temperature ionic liquids (ILs), considered as the "designer solvent", is the subject of numerous studies, because its properties can be modified by various combinations of organic cations and organic/inorganic anions, as well as by the introduction of different functional groups on the ions. To date, ILs have attracted significant attention as a new type of electrolyte of supercapacitors, because of their low volatility, high ionic conductivity, and wide electrochemical window that can deliver an energy density comparable to that of the lead-acid battery. A well understanding of the electric double layer (EDL) of this new type electrolyte is a prerequisite to the design of a supercapacitor with good performance. Up to now, the interfacial EDL structure of IL has been studied by theoretical, experimental[1-7] and computational methods[8-15] Differential capacitance (C_d), as an experimentally accessible quantitative measurement of the response of EDL structure to a change in electrode potential, has been widely used to investigate the properties of IL/electrode interface.[2, 14, 16]

The traditional Helmholtz model, with a constant value of capacitance, is not suitable for describing the EDL structure of IL/electrode system, while the Gouy-Chapman theory with U-shaped differential capacitance-potential (C_d-U) curves for dilute electrolytes is also expected cannot describe the IL interfacial structure due to the solvent-free nature and the finite size of ILs. Given the finite size of ions in ILs, several analytical mean-field theories[10-11] have been proposed to describe the EDLs in concentrated ionic systems. Two types of C_d-U curves, i.e., the bell-shaped and camel-shaped C_d-U curves were predicted, also, the two different C_d-U curves were observed in experiments.[2] However, as the IL/electrode interface is highly complicated due to the complicated electrode/electrolyte interactions and ionic correlations,

molecular dynamics (MD) simulation is a powerful technique for studying the IL/electrode interface at the molecular level.

In our previous computational[17, 18] and experimental[19] studies, it has been demonstrated that there is specific adsorption of imidazolium (im) cation from the π-stacking interaction between the aromatic im-ring and the sp^2 graphite surface. The goal of the current work is to study the influences of repulsive interactions, characterized by the parameter of λ, between the graphite surface and the $BMIM^+/PF_6^-$, on the structure of EDL and C_d by using molecular dynamics simulation. The C_d value of $BMIM^+/PF_6^-$ /graphite system, as λ is in the range of 1.00 to 0.25, is found higher at the negative polarization than that at the positive polarization. Such trend is due to the thinner thickness of EDL, resulting from the dominant role of the specific adsorption of the $BMIM^+$, compared with the repulsive interactions, while the situation is opposite when λ is 0.05. Apart from that, the maximum of C_d decrease with increasing the repulsions at the negative polarization, attributed to the elongated thickness of EDL. However, the maximum of C_d at the positive polarization is slight complex. When λ changes from 1.00 to 0.75, the maximum of C_d increase marginally, and then it decreases from λ=0.75 to 0.05 as cases at the negative polarization. Detailed analysis of EDL structure based on anatomy of the number density profiles and orientational ordering are described below. In addition, how to exert different repulsive interactions between graphite electrode and $BMIM^+/PF_6^-$ is described in the Computational methods.

2. Computational methods

We performed molecular dynamics simulations of pure $BMIM^+/PF_6^-$ IL between two oppositely charged electrodes, composed of frozen graphene layers on both sides of the simulation cell, and the separation between the two inner graphene layers was set to be 100 Å, allowing the EDL and the differential capacitance on the two oppositely charged walls to be studied separately.[13] The simulation process is similar to our previous studies.[17, 18] Briefly, the $BMIM^+/PF_6^-$ bulk phases contain 439 cation-anion pairs for all systems (i.e. the overall number density of all systems was identical for clearer comparison) and these systems were run at 450 K under 1 bar. The force field parameters are taken from Pádua's work,[20] and the carbon atoms of the graphite (0001) surface interact with $BMIM^+/PF_6^-$ via the Lennard-Jones potential corresponding to the sp^2 hybrid carbon atoms in the AMBER force field.[21] Strictly, it is not appropriate to model the specific adsorption caused by π-stacking using the classical Lennard-Jones potential. On the other hand, it is notable that our simulated results were in good agreement with that of the microscopic adsorption structures of the same ionic liquid on graphene by Ghatee et al[22]. using *ab initio* calculations. Thus, it is practical to estimate the role of specific adsorption caused by π-stacking by scaling Lennard-Jones interaction with classical MD simulations. The van der Waals and the real space electrostatic interaction cutoff distance is set to be 12 Å, and the smoothed particle-mesh Ewald (SPME) algorithm[23] elongated up to 700 Å in z direction (i.e. the direction perpendicular to the graphite electrode surface) is used to handle the long-range electrostatic interactions in reciprocal space, whilst a slab correction[24] is induced along the z direction for such an essential two-dimensional periodic system along the xy-directions. For each system, 11 MD runs were performed with a fixed charge density σ on the two inner graphene layers in the internal from -11 to +11 μC cm^{-2}, with an increment of 1 μC cm^{-2}. Charges with opposite signs were put on the carbon sites of the two inner graphene layers in contact with the $BMIM^+/PF_6^-$, so that the whole system was charge neutral. For each simulation, after initial annealing from 1000 to T K within 20 ns, a trajectory of 50 ns was gradually generated at 450 K, coupled to a Nosé-Hoover-chain thermostat[25, 26] to generate a converged EDL because dynamics of IL was slow.[27, 28] The integration time step was 2 fs with a SHAKE/RATTLE algorithm[29, 30] applied on constraining all the C-H bonds. The simulation was performed with a home-made MD package and the image charges were not considered in the current work. To explore the interaction between ions and electrodes, we use Lennard–Jones potential of $u(r;\lambda) = 4\varepsilon[(\sigma/r)^{12}-\lambda(\sigma/r)^{6}]$,[31] tunable by varying a control parameter λ.

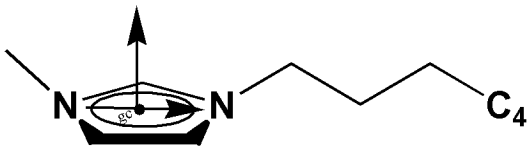

Scheme 1. The structure of 1-butyl-3-methyl-imidazolium ($BMIM^+$); the im-ring geometrical center of $BMIM^+$, butyl head carbon of $BMIM^+$, denoted as gc and C_4; im-ring normal of $BMIM^+$ and nitrogen-nitrogen vector on the im-ring of $BMIM^+$

3. Results and Discussions

3.1 Effects of repulsive interactions on C_d

Fig. 1(a) illustrated the relation between the simulated electrode surface charge density (σ) and the electrode potential (U) of $BMIM^+/PF_6^-$/graphite at five different repulsions of λ = 1.00, 0.75, 0.50, 0.25 and 0.05, respectively. The case of λ=1.00, means the normal Lennard-Jones interaction between the $BMIM^+/PF_6^-$ IL and the graphite electrode. Notably, the repulsive interaction increases with decreasing the value of λ, that is, when λ is 0.05, the repulsion is the strongest. The σ-U curves were fitted segmentally by polynomials and were connected by error functions.[32] Accordingly, C_d-U curves under the above five repulsive interactions, shown in Fig. 1(b), were obtained by differentiating the fitted σ-U curves.

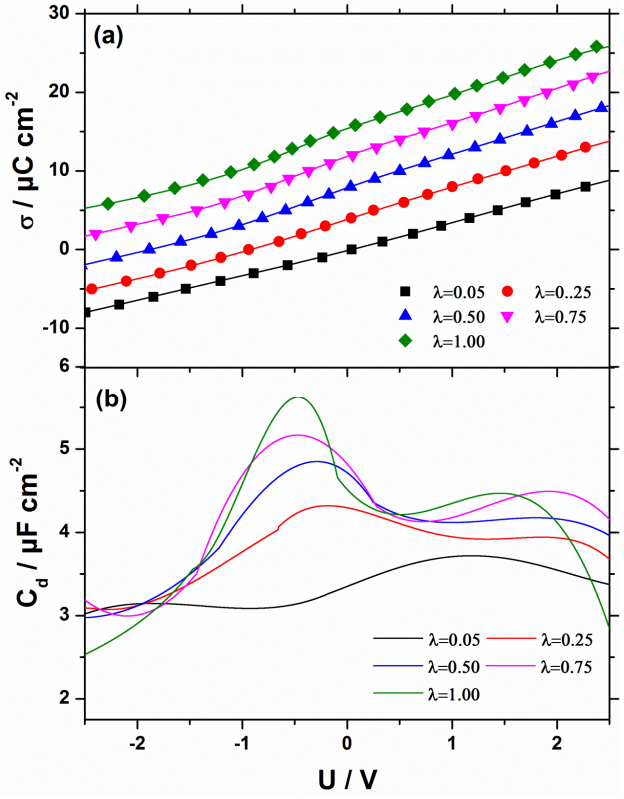

Fig. 1 (a) Surface charge density (*σ*) versus electrode potential (*U*) for $BMIM^+/PF_6^-$ at λ=1.00, 0.75, 0.50, 0.25 and 0.05 at 450 K, and an increment of 4 μC cm^{-2} was successively added to the data of λ=1.00, 0.75, 0.50 and 0.25 to distinguish them as guide to eyes. The lines in (a) are fitted to *σ – U* relation at individual repulsions, (b) Differential capacitance (C_d) of $BMIM^+/PF_6^-$ IL as a function of electrode potential at λ=1.00, 0.75, 0.50, 0.25 and 0.05, respectively.

Several features can be seen from Fig. 1(b): (1) all C_d-U curves for $BMIM^+/PF_6^-$/graphite at five repulsions are asymmetric camel-shaped, with potential of zero charge (PZC) at 0.084, 0.052, 0.032, 0.039 and 0.043 V, at λ of 1.00, 0.75, 0.50, 0.25 and 0.05, respectively. (2) When λ is in the range of 0.25 to 1.00, C_d at the negative polarization are higher than that at the positive polarization, due to the dominant role of specific adsorption of $BMIM^+$ as compared with the repulsive interaction. Such adsorption is caused by the π-stacking between the aromatic im-ring and sp^2 graphite electrode surface, which has been demostrated by our previous studies.[17, 19, 33] But for the case of λ = 0.05, the trend is opposite, because the specific adsorption is greatly weakened, and the smaller size of anion as compared to the cation dominates in determining the effective thickness of EDL. (3) The maximum of C_d monotonically decrease with increasing repulsive interactions at the negative polarization, induced by the larger effective thickness of EDL, while the situation is marginally complicated at the positive polarization. Specifically, the maximum of C_d first increase slightly at the positive polarization when small repulsion is exerted by changing λ from 1.00 to 0.75, which can be understood as the weakened specific adsorption of cations, and thus allows more effective screening of anions to the electrode surface charge. And then they decrease with the increase of repulsions from λ=0.75, due to the larger effective thickness of EDL. Thus, it is desirable to a close inspect on the effects of competition between the repulsive interaction and the specific adsorption of $BMIM^+$ on EDL structure at both positive and negative polarizations, as will be discussed below.

3.2 Density profiles of ions at different repulsive interactions

Influences of repulsive interactions between $BMIM^+/PF_6^-$ and the graphite electrode on the EDL structure of $BMIM^+/PF_6^-$/graphite is investigated by analyzing the number density profiles, ρ(z), of the geometrical center of the im-ring of $BMIM^+$, the butyl head carbon of $BMIM^+$, (cf. gc and C_4 denoted in Scheme 1) and the center-of-mass of PF_6^- at surface charge densities of σ = 0 μC cm^{-2}, ±2 μC cm^{-2} and ±6 μC cm^{-2} at λ = 1.00, 0.75, 0.50, 0.25 and 0.05, respectively. The electrode potentials of the C_d maximum approximately correspond to surface charge densities of σ = -2 μC cm^{-2} and σ = 6 μC cm^{-2}. The density profiles between two neutral electrodes of σ = 0 μC cm^{-2} is symmetric, which is an important symbol to check whether the MD simulation time is long enough in order to ensure statistically averaged results, as shown in the top row of Fig. 2. It can be seen that the density oscillation extends several tens of angstroms into the bulk as a consequence of the overscreening effect.[34] It can also be observed that all the peak values of ρ(z) decrease and dramatically shift away from the electrode surface with the increasement of the repulsive interaction, indicating a less structural EDL at higher repulsions, and thus, the smaller C_d caused by the thicker EDL.

A remarkable feature that the gc of im-ring keeps close contact to

Journal Name RSCPublishing

ARTICLE

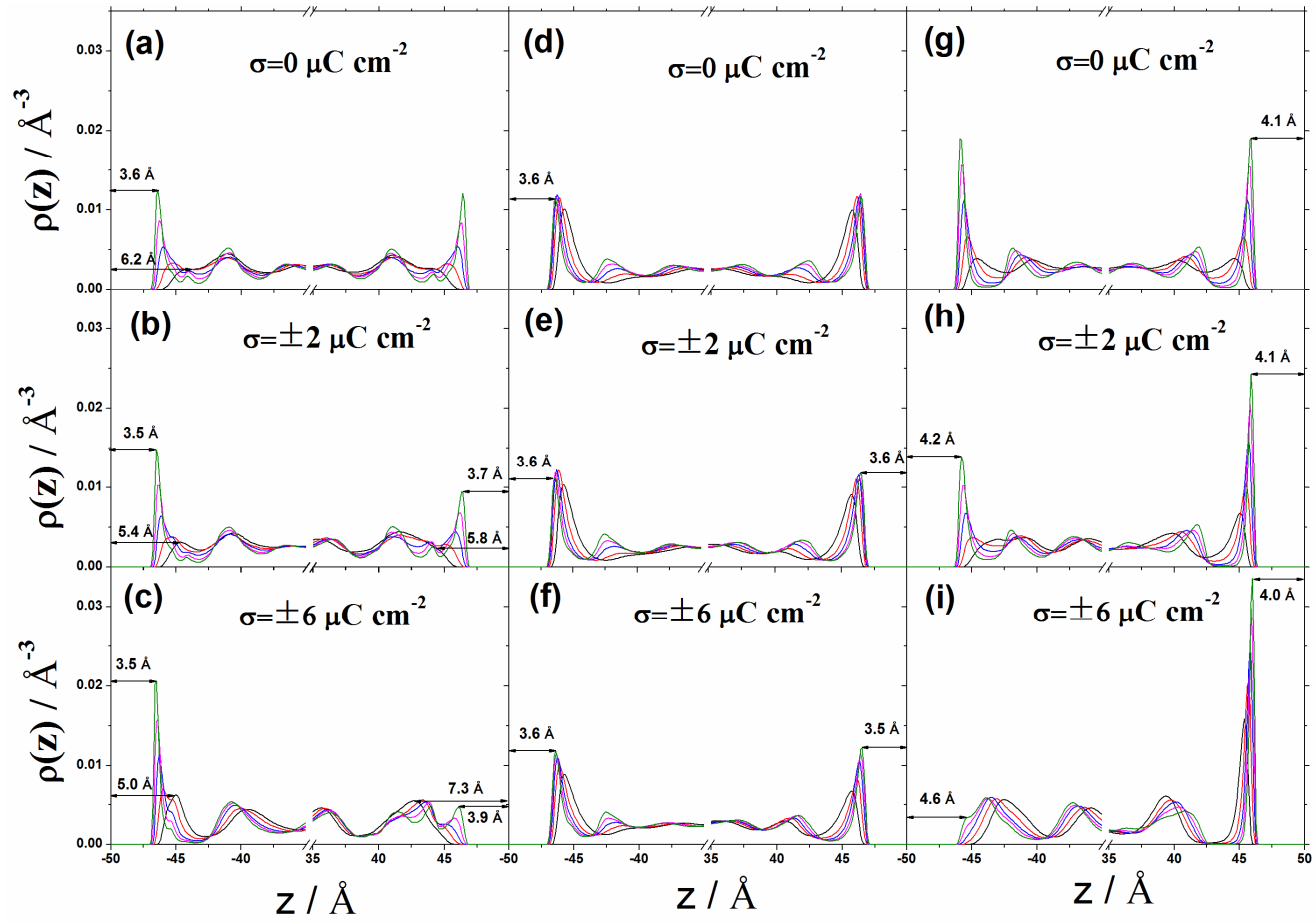

Fig. 2. Number density profiles of the gc of im-ring of $BMIM^+$, C_4 of $BMIM^+$, and center-of-mass position of PF_6^- for $BMIM^+/PF_6^-$ under the electrode surface densities of 0 μC cm^{-2} (a, d, g), ±2 μC cm^{-2} (b, e ,h) and ±6 μC cm^{-2} (c, f, i) at λ=1.00(green lines), 0.75(pink lines), 0.50(blue lines), 0.25(red lines) and 0.05(black lines), respectively. The two electrodes locate at -50 Å (neutral or negatively charged) and +50 Å (neutral or positively charged), respectively.

neutral and negatively charged electrode when there is no repulsive interaction, as displayed in Fig. 2a, 2b and 2c. This is reasonable because the positive charge on the $BMIM^+$ cation is mostly distributed on the im-ring. Successively increasing σ from 0 to -2 μC cm^{-2}, the first peak of the gc of im-ring shifts from z = 3.6 to 3.5 Å. And ρ(z) increases from nearly 0.0125 to 0.0149 $Å^{-3}$ for λ =1.00 and 0.0025 to 0.0031 $Å^{-3}$ for λ = 0.05, respectively. The overall increased accumulation is around 1.2 for the five repulsions. In Fig. 2c, we can see that the gc of $BMIM^+$ is expelled away from the electrode surface at the positive polarization of σ = 6 μC cm^{-2} and its peak appeared at 3.9 Å with much lower ρ(z) of less than 0.005 $Å^{-3}$ at λ = 1.00. As for the ρ(z) of C_4 atom of $BMIM^+$, it does not undergo such drastic enhancement or depression as σ switches from 0 to ±6 μC cm^{-2} when λ changes from 1.00 to 0.25, as depicted in the middle column of Fig. 2. Notably, peaks of C_4 atom of σ = ±6 μC cm^{-2} locates at 3.6 Å at the negative polarization and 3.5 Å at the positive polarization without repulsive interaction, that is, a closer contact to the electrode compared to that of 3.6 Å to a neutral electrode. The right column of Fig. 2 shows the ρ(z) of the center-of-mass of PF_6^-. For PF_6^-, ρ(z) at the positive polarization increases from nearly 0.019 to 0.034 $Å^{-3}$ for λ = 1.00 and 0.004 to 0.016 $Å^{-3}$ for λ = 0.05, respectively, and it is in a closer contact with the electrode, as expected. Moreover, PF_6^- is repelled much more strongly at the negative polarization, with the first peak position switching from 4.1 to 4.2 Å from σ = 0 μC cm^-

^{2} to σ = -2 μC cm^{-2}, and the first peak position of PF_6^- even located at 4.6 Å from the electrode as the charge density is increased to σ = -6 μC cm^{-2}.

3.3 Orientational distributions of BMIM$^+$ at different repulsive interactions

In order to further illustrate the effect of repulsion on ionic orientations at the graphite surface, the orientational distributions of BMIM$^+$ at λ = 1.00, 0.75, 0.50, 0.25 and 0.05, respectively, are presented in Fig. 3 The orientational distribution is defined as the ensemble average of the second Legendre polynomial, i.e., $P_2(\theta) = \langle(3\cos^2(\theta)-1)/2\rangle$,[18] where θ is the angle between the normal direction vector of the im-ring (cf. Scheme 1) and the electrode surface normal (z) or between the nitrogen-nitrogen (NN) vector on the im-ring (cf. Scheme 1) and z. The fact that $P_2(\theta)$, shown in Fig. 3a, for λ changes from 1.00 to 0.75 in the innermost layer approximate unit, accompanied by the values of $P_2(\theta)$ approximating -0.5 in Fig. 3d, indicates that the im-ring of the BMIM$^+$ in the first layer tends to orient parallel to the uncharged electrode surface under different repulsive interactions due to the π-stacking interaction.[17, 19]. It is notable that such feature persists even at positively charged electrode at σ = 6 μC cm^{-2}, as shown in Fig. 3c and 3f. As increasing the repulsive interaction, not only the BMIM$^+$ is expelled from the electrode surface, shown in Fig. 2, but their orientation become more random in the first layer, as indicated in Fig. 3a. Interestingly, the overall orientational distributions of BMIM$^+$, both on the negatively charged electrode and the positively charged electrode, are broader with the increasement of the repulsion, implying the less structural feature, as distributions of ρ(z) in Fig. 2.

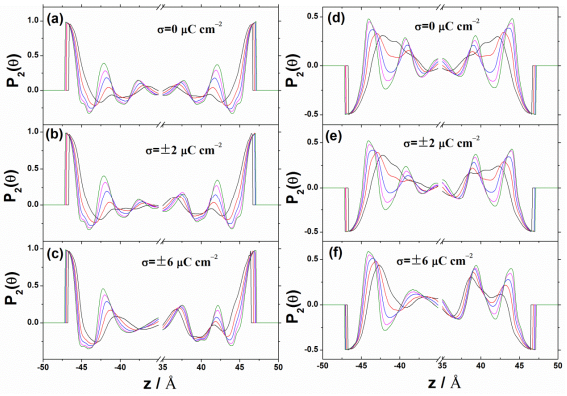

Fig. 3. Orientational ordering, $P_2(\theta)$, of the BMIM$^+$ im-ring normal, along the surface normal direction z of the electrode under the electrode surface densities of 0 μC cm^{-2} (a), ±2 μC cm^{-2} (b) and ±6 μC cm^{-2} (c), or between the nitrogen-nitrogen vector on the im-ring of BMIM$^+$ and z under the electrode surface densities of 0 μC cm^{-2} (d), ±2 μC cm^{-2} (e) and ±6 μC cm^{-2} (f), at λ=1.00, 0.75, 0.50, 0.25 and 0.05, respectively.

When λ=1.00, both the first peak of ρ(z) locate at 3.6 Å to the uncharged electrode surface shown in Fig. 2a and 2d, as well as the parallel alignment of im-ring on the graphite surface delineated in Fig. 3a and 3d, it can be deduced that the BMIM$^+$ tends to lie flat on the uncharged electrode surface, as reported in our previous studies.[17, 19] Upon charging to σ = -2 μC cm^{-2}, such flat configuration switches to a slant configuration with C_4 in closer contact with the negatively electrode surface, as can be observed from the positions of the first ρ(z) peak and the values of $P_2(\theta)$. Specifically, distances of the first ρ(z) peak of gc and C_4 to the negatively charged electrode of σ = -2 μC cm^{-2} are 3.5 Å, 3.6 Å for λ=1.00, 3.6 Å, 3.6 Å for λ=0.75, 3.8 Å, 3.7 Å for λ=0.50, 4.7 Å, 3.9 Å for λ=0.25 and 4.3 Å, 5.3 Å for λ=0.05, respectively, accompanied with the corresponding $P_2(\theta)$ values of 0.9107, 0.8912, 0.8386, 0.2741 and 0.1875. However, the slant configuration with gc in closer contact with the negatively charged electrode, switches to a parallel conformation when λ=0.75, and this conformation turns to be slant with C_4 in closer contact when increasing repulsions. On the other hand, upon charging from σ =0 μC cm^{-2} to σ =6 μC cm^{-2}, the BMIM$^+$ is inclined to switch from a flat configuration to a slant configuration with C_4 in closer contact with the positively charged electrode under different repulsive interactions, as presented in Fig. 2a, c and f.

3.4 Competitive effects of specific adsorption of BMIM$^+$ and the repulsive interaction on the EDL structure

Combined with the previous studies of the specific adsorption of BMIM$^+$ that can shorten the thickness of EDL,[17, 19] as well as the analyses of the density profiles and orientational ordering, effects of the competition between the repulsive interaction and the specific adsorption on the EDL structure is clear. Specifically, when the repulsive interaction is larger, the smaller C_d is obtained, due to the larger effective thickness of EDL that can be observed from the broadening of the density profiles and the orientational distributions of BMIM$^+$, shown in Fig. 2 and Fig. 3. Though the repulsive interaction has a significant role in expelling the BMIM$^+$ away from the negatively electrode surface that induces the monotonical decrease of C_d, the specific adsorption of BMIM$^+$ is still the dominant factor in determining the overall EDL structure until λ=0.05, verified by the higher C_d at the negative polarization than that at the positive polarization when λ is larger than 0.05, as shown in Fig. 1b. However, such specific adsorption of cations raises the electrode potential on the positively charged electrode and depresses the C_d at the positive polarization. the BMIM$^+$ lie flat on the neutral electrode surface. Such parallel alignment of BMIM$^+$ in the

innermost layer at the charge density of -2 μC cm^{-2} firstly switches to slant configuration with gc in closer contact with the electrode when λ>0.75, and then it lie flat on the surface when λ=0.75. Subsequently, it evolves to a slant configuration with C_4 in closer contact with the negatively charged electrode when λ<0.75. On the other hand, the flat configuration of $BMIM^+$ on the neutral electrode switches to a slant configuration with C_4 in closer contact with the positively charged electrode.

With these two competitive effects at the positive polarization, the C_d do not decay monotonically as that at the negative polarization. And influences of the specific adsorption of $BMIM^+$ and the repulsive interaction on EDL at the positive polarization is slight complex. Specifically, the small enhanced C_d at λ=0.75, shown Fig. 1b, is caused by the weakened specific adsorption of $BMIM^+$ with increasing repulsion, allowing more effective screening of the positively charged electrode by PF_6^-. Apart from that, a thicker EDL with the increasing repulsion can also apply on the positive polarizations, which depresses C_d when λ<0.75.

3.5 Molecular insights into the arrangement of $BMIM^+$ in the innermost layer

The arrangement of $BMIM^+$ in the innermost layer at different repulsions is shown in Fig. 4. The innermost layer is taken to be the first valley of the number density profiles of the gc of the im-ring of $BMIM^+$ in Fig. 2. The in-plane organization of $BMIM^+$ can be observed at stronger specific adsorption, in line with the $P_2(\theta)$ values between the $BMIM^+$ im-ring normal (approximate unit, shown in Fig. 3a-c) or the nitrogen-nitrogen vector on the im-ring of $BMIM^+$ and *z* direction (approximate -0.5, shown in Fig. 3d-f). Clearly, the effective thickness of EDL at the negative polarization is thinner than that at the positive polarization. Such an effect is manifested in the differential capacitance, with a higher value on the negative polarization branch than on the positive polarization branch, shown in Fig. 1b. It is also remarkable that the larger the repulsions, the thicker EDL under the same charge density of both neutral (Fig. 4 a-c and g-i) and charged electrode (Fig. 4 d-f and j-l), in good agreement with the broadening of the density profiles and the orientational distributions of $BMIM^+$ in Fig. 2 and Fig. 3. Apart from that, the parallel configuration of $BMIM^+$ switches to a slant configuration when repulsion is increased.

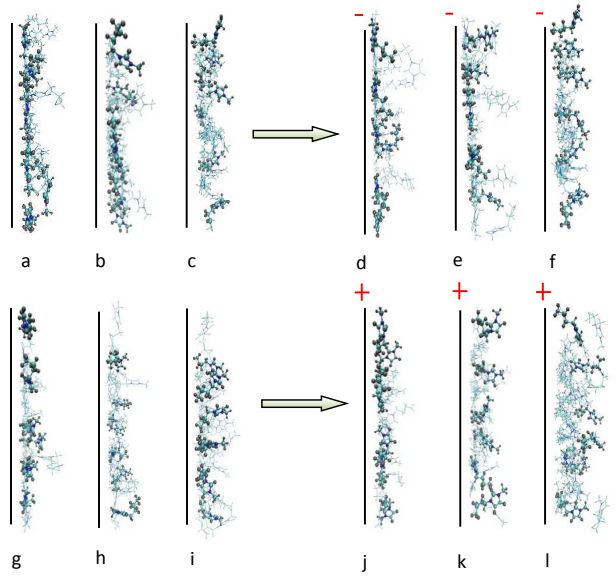

Fig. 4. Representative snapshots of the $BMIM^+$ at σ=0 μC/cm^2 (a-c and g-i), σ= -6 μC/cm^2 (d-f) and σ=6 μC/cm^2 (j-l) at three different repulsions of λ=1.00 (a, d, g, j), 0.50 (b, e, h, k) and 0.05 (c, f, I, l), respectively.

4. Conclusion

Strength of the repulsive interaction on EDL structure of $BMIM^+/PF_6^-$/graphite is studied by MD simulations. All C_d-U curves are asymmetric camel-shaped. When 0.25<λ<1.00, C_d at the negative polarization is larger than that at the positive polarization due to the thinner effective thickness of EDL contributed by the specific adsorption of $BMIM^+$. The situation is opposite when λ=0.05 caused by the thicker EDL under the strongest repulsive interactions. Apart from that, the monotonical decrease of C_d maximum at the negative polarization can be ascribed to the increase of the repulsive interactions that can expel ions away from the electrode and thus elongate the EDL, while it firstly increase the C_d at the positive polarization when λ changes from1.00 to 0.75 by allowing more effective screening of PF_6^-, and then it decreases as the repulsive interaction increases. The overall variation of EDL of $BMIM^+/PF_6^-$/graphite can be attributed to the competition between the repulsive interaction and the specific adsorption of $BMIM^+$.

Acknowledgements

This work was supported by NSFC (21373118, 21073097, 21203100, 21421001), the Natural Science Foundation of Tianjin (12JCYBJC13900, 13JCQNJC06700), and the MOE Innovation Team (IRT13022) of China. The simulations were performed on TianHe-1(A) at the National Supercomputer Center in Tianjin.

Notes and References

[a]*Tianjin Key Laboratory of Metal- and Molecular-Based Material Chemistry, Key Laboratory of Advanced Energy Materials Chemistry (Ministry of Education), Collaborative Innovation Center of Chemical Science and Engineering (Tianjin), Institute of New Energy Material Chemistry, College of Chemistry, Nankai University, Tianjin 300071, People's Republic of China*

**email address: tyan@nankai.edu.cn*

† Authors W. Y. Jin and X. H. Liu contributed equally.

‡Present address: Department of Chemistry, University of Chicago, 5735 South Ellis Avenue, Chicago, Illinois 60637, Unites States of America

1 M. T. Alam, J. Masud, M. M. Islam, T. Okajima and T. Ohsaka, *J. Phys. Chem. C*, 2011, **115**, 19797-19804.

2 V. Lockett, R. Sedev, J. Ralston and M. Horne, *J. Phys. Chem. C*, 2008, **112**, 7486-7495.

3 Y. Z. Su, Y. C. Fu, J. W. Yan, Z. B. Chen and B. W. Mao, *Angew. Chem. Int. Ed.*, 2009, **48**, 5148-5151.

4 V. Lockett, M. Horne, R. Sedev, T. Rodopoulos and J. Ralston, *Phys. Chem. Chem. Phys.*, 2010, **12**, 12499-12512.

5 Y. Z. Su, Y. C. Fu, Y. M. Wei, J. W. Yan and B. W. Mao, *ChemPhysChem*, 2010, **11**, 2764-2778.

6 M. V. Fedorov and A. A. Kornyshev, *Chem. Rev.*, 2014, **114**, 2978-3036.

7 R. Burt, G. Birkett and X. S. Zhao, *Phys. Chem. Chem. Phys.*, 2014, **16**, 6519-6538.

8 M. Sha, Q. Dou, F. Luo, G. Zhu and G. Wu, *ACS Appl. Mater. Inter.*, 2014, **6**, 12556-12565.

9 A. A. Kornyshev, *J. Phys. Chem. B*, 2007, **111**, 5545-5547.

10 K. B. Oldham, *J. Electroanal. Chem.*, 2008, **613**, 131-138.

11 Y. Han, S. Huang and T. Yan, *J. Phys.: Condens. Matt.*, , 2014, **26**, 284103.

12 A. A. Kornyshev, N. B. Luque and W. Schmickler, *J. Solid State Electrochem.*, 2014, **18**, 1345-1349.

13 G. Feng, J. S. Zhang and R. Qiao, *J. Phys. Chem. C*, 2009, **113**, 4549-4559.

14 J. Vatamanu, O. Borodin and G. D. Smith, *J. Am. Chem. Soc* 2010, **132**, 14825-14833.

15 M. Armand, F. Endres, D. R. MacFarlane, H. Ohno and B. Scrosati, *Nat. Mater.*, 2009, **8**, 621-629.

16 S. Baldelli, *Acc. Chem. Resear.*, 2008, **41**, 421-431.

17 X. J. Si, S. Li, Y. L. Wang, S. H. Ye and T. Y. Yan, *ChemPhysChem*, 2012, **13**, 1671-1676.

18 S. Wang, S. Li, Z. Cao and T. Yan, *J. Phys. Chem. C*, 2010, **114**, 990-995.

19 Q. Zhang, Y. N. Han, Y. L. Wang, S. H. Ye and T. Y. Yan, *Electrochem. Commun.*, 2014, **38**, 44-46.

20 J. N. Canongia Lopes, J. Deschamps and A. A. H. Pádua, *J. Phys. Chem. B*, 2004, **108**, 2038-2047 Addions and Corrections: ibid. 2004, 2108,11250-11250.

21 W. D. Cornell, P. Cieplak, C. I. Bayly, I. R. Gould, K. M. Merz, J. Ferguson, M. David, D. C. Spellmeyer, T. F. Caldwell, W. James and A. K. Peter, *J. Am. Chem. Soc.*, 1995, **117**, 5179-5197

22 M. H. Ghatee and F. Moosavi, *J. Phys. Chem. C*, 2011, **115**, 5626-5636.

23 U. Essmann, L. Perera, M. L. Berkowitz, T. Darden, H. Lee and L. G. Pedersen, *J. Chem. Phys.*, 1995, **103**, 8577-8593.

24 I. Yeh and M. L. Berkowitz, *J. Chem. Phys.*, 1999, **111**, 3155-3162.

25 G. J. Martyna, M. L. Klein and M. Tuckerman, *J. Chem. Phys.*, 1992, **97**, 2635-2643.

26 G. J. Martyna, M. E. Tuckerman, D. J. Tobias and M. L. Klein, *Mol. Phys.*, 1996, **87**, 1117-1157.

27 T. Yan, Y. Wang and C. Knox, *J. Phys. Chem. B*, 2010, **114**, 6886-6904.

28 T. Yan, Y. Wang and C. Knox, *J. Phys. Chem. B*, 2010, **114**, 6905-6921.

29 J. Ryckaert, G. Ciccotti and H. J. C. Berendsen, *J. Comput. Phys.*, 1977, **23**, 327-341.

30 H. C. Andersen, *J. Comput. Phys.*, 1983, **52**, 24-34.

31 A. Waghe, J. C. Rasaiah and G. Hummer, *J. Chem. Phys.*, 2002, **117**, 10789-10795.

32 N. Georgi, A. A. Kornyshev and M. V. Fedorov, *J.*

Electroanal. Chem., 2010, **649**, 261-267.

33 X. Liu, Y. Han and T. Yan, *ChemPhysChem*, 2014, **15**, 2503-2509.

34 M. V. Fedorov, N. Georgi and A. A. Kornyshev, *Electrochem. Commun.*, 2010, **12**, 296-299.